Flux-induced semiconducting behavior of a quantum network

Shreekantha Sil,[1] Santanu K. Maiti,[2] and Arunava Chakrabarti[3]
[1]*Department of Physics, Visva-Bharati, Santiniketan, West Bengal 731 235, India*
[2]*Department of Physics, Narasinha Dutt College, 129 Belilious Road, Howrah 711 101, India*
[3]*Department of Physics, University of Kalyani, Kalyani, West Bengal 741 235, India*
(Received 3 April 2009; published 19 May 2009)

We show that a diamond-shaped periodic network, recently proposed as a model of a spin filter [A. Aharony, O. Entin-Wohlman, Y. Tokura, and S. Katsumoto, Phys. Rev. B **78**, 125328 (2008)], is capable of behaving as a *p*-type or an *n*-type semiconductor depending on a suitable choice of the on-site potentials of the atoms occupying the vertices of the lattice and the strength of the magnetic flux threading each plaquette of the network. A detailed study of the density of states of an infinite network is made together with the conductance of finite-sized system to establish the idea.

DOI: 10.1103/PhysRevB.79.193309 PACS number(s): 64.60.aq, 63.22.−m, 63.50.−x

Low-dimensional model quantum systems have been the objects of intense research, both in theory and in experiments, mainly due to the fact that these simple-looking systems are prospective candidates for nanodevices in electronic as well as spintronic engineering.[1–15] Apart from this feature, several striking spectral properties are exhibited by such systems owing to the quantum interference which is specially observed in quantum networks containing closed loops. Examples are the Aharonov-Bohm (AB) effect[5] in the magnetoconductance of quantum dots,[7] electron transport in quantum-dot arrays,[3,4] Fano effect in a quantum ring-quantum dot system,[8] spin-filter effects in mesoscopic rings,[10,11] and dots[6] to name a few.

Recently, Aharony *et al.*[1,2] proposed a model of a nanospintronic device using a linear chain of diamondlike blocks of atomic sites. Each plaquette of the array is threaded by identical magnetic flux. They have analyzed how the Rashba spin-orbit interaction and the AB flux combine to select a propagating ballistic mode. A similar chain was earlier investigated by Bercioux *et al.*[12,13] in the context of spin-polarized transport of electrons and by Vidal *et al.*[14] and Doucot and Vidal[15] to study two interacting particles,[14] and Josephson-junction chain of diamonds,[15] both in the presence of a magnetic field. However, there are certain special spectral features offered by the diamond chain, particularly, the role of the AB flux, which we believe, remain unexplored. This is precisely the area we wish to highlight in the present communication. We show that an infinite diamond chain of identical atoms behaves as an insulator at $T=0$ K in the presence of a nonzero AB flux. As we arrange atoms of two different kinds (represented by two different values of the on-site potential) periodically on a diamond chain, a highly degenerate localized level is created near one of the two subbands of extended states. The proximity of this localized level to either of the subbands can be controlled by tuning the AB flux and can be made to stay arbitrarily close to either of the subbands. The entire system is then capable of behaving as an *n*-type or a *p*-type semiconductor as explained later. The conductance spectrum of a finite array of the diamond plaquettes is also studied to judge the applicability of such a network geometry in device engineering.

We adopt a tight-binding formalism and incorporate only the nearest-neighbor hopping. We begin by referring to Fig. 1(a). A magnetic (AB) flux ϕ threads each plaquette. The Hamiltonian of the network is given by

$$H = \sum_i \epsilon_i c_i^\dagger c_i + \sum_{\langle ij \rangle} t(c_i^\dagger c_j e^{i\theta_{ij}} + c_j^\dagger c_i e^{-i\theta_{ij}}), \tag{1}$$

where $c_i(c_i^\dagger)$ are the annihilation (creation) operator at the ith site of the network, ϵ_i is the on-site potential at the ith site which we shall choose as ϵ_A or ϵ_B as shown and t is the constant nearest-neighbor hopping integral. The phase θ_{ij} is constant and is given by $\theta_{ij}=\pm 2\pi\phi/4\phi_0$, where $\phi_0=hc/e$ is the flux quantum. The positive or negative sign of the phase factor depends on whether the electron hops from site $A(B)$ to site $B(A)$ *along the arrow* (called the "forward" hopping) or against it ("backward" hopping).

To obtain the average density of states (AVDOS) of the infinite system we make use of the system of equations satisfied by the Green's function G_{ij}, viz.,

$$(E-\epsilon_i)G_{ij} = \delta_{ij} + t\sum_k e^{i\theta_{ik}} G_{kj}. \tag{2}$$

On the right-hand side of Eq. (2) the index k runs over the nearest neighbors of the ith site. The density of states is obtained by a decimation renormalization-group (RG) method.[16] The RG scheme is depicted in Fig. 1. The lower A vertices in Fig. 1(a) are decimated first, and the original diamond array gets transformed into an array of triangular plaquettes with the surviving A atoms sitting at the top and

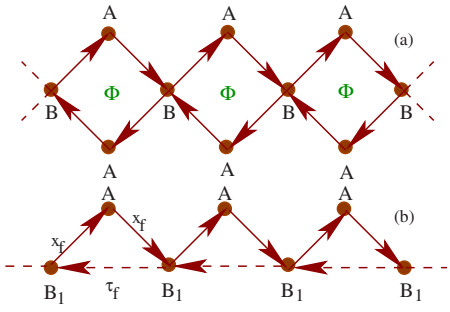

FIG. 1. (Color online) (a) Schematic view of a section of an infinite diamond chain. (b) The RG scheme. The arrow gives the direction of the *forward* hopping $t\exp(i\theta_{ij})$.

the pair of original B atoms getting renormalized into a pair of B_1 atoms, each characterized by the effective on-site potential $\epsilon_{B_1}=\epsilon_B+2t^2/(E-\epsilon_A)$. The B_1-B_1 effective hopping integral is $\tau_f=t^2\exp(i\pi\phi/\phi_0)/(E-\epsilon_A)$, and its complex conjugate $\tau_b=\tau_F^*$. $x_f=t\exp(i\pi\phi/2\phi_0)$ is the B_1-A hopping integral as shown in Fig. 1(b). Its conjugate is named x_b. The subscripts $'f'$ and $'b'$ refer to the *forward* or *backward* hopping due to the broken time-reversal symmetry due to the magnetic flux. In Fig. 1(b) we have not shown the flux explicitly as the flux has been automatically included in x_f, x_b, τ_f, and τ_b. The array of triangles is now renormalized by decimating the alternate A sites and the appropriate B sites preserving the triangular geometry of the array. The recursion relations satisfied by the parameters are given by

$$\epsilon_A' = \epsilon_A + p_2 x_b + p_1 x_f,$$

$$\epsilon_{B_1}' = \epsilon_{B_1} + 2\frac{x_f x_b}{E-\epsilon_A} + h_f r_1 + h_b r_2 \tag{3}$$

for the site potentials and

$$x_f' = h_b p_2; \quad \tau_f' = h_f q_1 \tag{4}$$

for the hopping integrals between B_1-A and B_1-B_1 pairs on the renormalized triangular array. Obviously, x_b' and τ_b' are given by $x_f'^*$ and $\tau_f'^*$, respectively, and $p_1=[x_b(E-\epsilon_2)+x_f\tau_f]/\delta$, $p_2=p_1^*$, $h_f=\tau_f+x_b^2/(E-\epsilon_A)$, $h_b=h_f^*$, $r_1=[h_b(E-\epsilon_2)]/\delta$, and $r_2=r_1^*$ with $\epsilon_2=\epsilon_{B_1}+x_f x_b/(E-\epsilon_A)$ and $\delta=(E-\epsilon_2)^2-\tau_f\tau_b$. With a small imaginary part added to the energy E, the local Green's functions at the sites A and B of the original diamond array are then obtained as

$$G_{AA}=\frac{1}{E+i0^+-\epsilon_A^*}; \quad G_{BB}=\frac{1}{E+i0^+-\epsilon_{B_1}^*}, \tag{5}$$

where the superscript * above refer to the fixed-point values of the respective parameters. The AVDOS is given by

$$\rho(E)=\frac{2}{3}\rho_A(E)+\frac{1}{3}\rho_B(E), \tag{6}$$

where $\rho_i(E)=-(1/\pi)\mathrm{Im}\,G_{ii}$, with i being A or B.

Let us now present two separate cases which will throw light on the central problem addressed in this Brief Report, viz., the semiconducting behavior of such a network.

Case I: $\epsilon_A=\epsilon_B$.

The AVDOS in this case is illustrated for $\epsilon_A=\epsilon_B=0$ in Figs. 2(a)–2(c) for $\phi=0$, for $\phi=\phi_0/5$, and for $\phi=2\phi_0/5$, respectively. In the zero flux case the spectrum is a continuum with a very high value of the density of states at the center, i.e., at $E=0$. The system exhibits a metallic character. As the magnetic field through the plaquette assumes nonzero value, a gap opens at the center with the peak in the AVDOS fixed at $E=0$. This high value of the AVDOS corresponds to strongly localized states. It is to be appreciated that these states are localized strictly on the A-type vertices of the array and the care has to be taken while renormalizing the diamond array so that both the A-type sites do not get decimated. This precise RG scheme is explained earlier. If the state corresponding to an energy E is localized then the

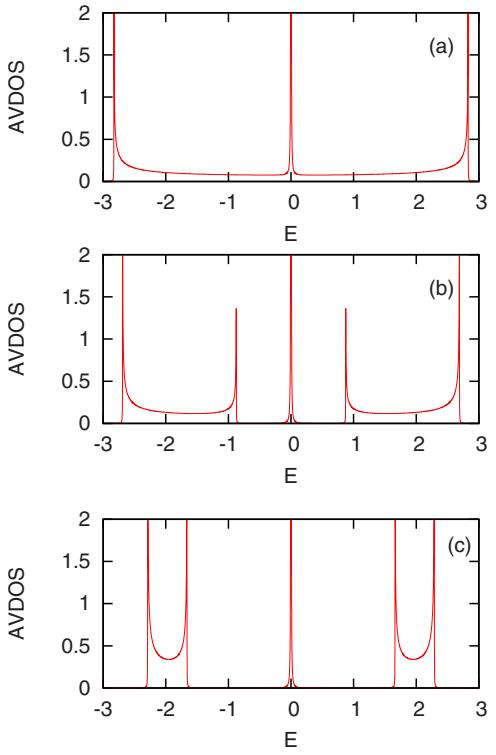

FIG. 2. (Color online) $\rho(E)$-E for an infinite diamond network array when the AB flux is (a) $\phi=0$, (b) $\phi=\phi_0/5$, and (c) $\phi=2\phi_0/5$. We have chosen $\epsilon_A=\epsilon_B=0$ and $t=1$. The AVDOS has been plotted within the range zero to two.

renormalized hopping integral will iterate to zero. This is observed for the central peak in the AVDOS by iterating Eq. (4). The gap around the central peak widens as the flux is increased gradually and the subbands at the two extremities shrink to two sharp lines of zero width as $\phi=\phi_0/2$. The picture reverses as ϕ increases from $\phi_0/2$ to ϕ_0. The exactly symmetrical location of the localized level with respect to the subbands at the flanks makes the system behave as a semiconductor when the electronic filling of the system lies between $\frac{1}{3}$ and $\frac{2}{3}$. More precisely, one can get a p-type semiconductor when the filling factor n_e is $\frac{1}{3}$ and an n-type semiconductor when $1/3<n_e\leq 2/3$.

Case II: $\epsilon_A\neq\epsilon_B$.

The AVDOS is exhibited in Fig. 3 with $\epsilon_B=0$ and $\epsilon_A=2$ for different values of the flux. By comparing Figs. 2 and 3 we see that the highly degenerate localized level is pinned at $E=\epsilon_A$. This has been verified using various values of ϵ_A keeping ϵ_B fixed. So the states are localized at the vertices A of the diamond chain. The other interesting feature is that as the gaps open up for nonzero flux, the localized level is placed asymmetrically with respect to the continuous subbands of extended eigenstates. With a proper tuning of the flux, one such subband can be brought arbitrarily close to the sharp-localized level. For example, with $\epsilon_A=2$, the localized level resides closer to the upper subband (the conduction band) than the lower one (the valence band). A reversal of the sign of the on-site potential ϵ_A reverses the picture. In either case, the localized level can be placed arbitrarily close to any one of the subbands by appropriately tuning the value

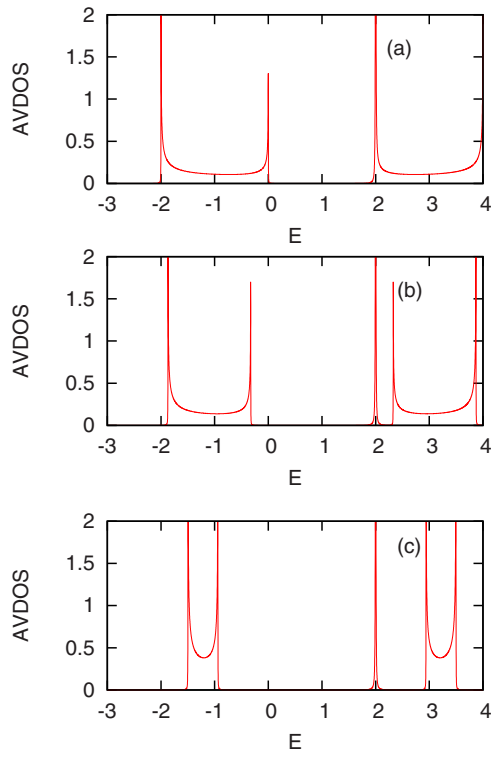

FIG. 3. (Color online) $\rho(E)$-E for an infinite diamond network array when the AB flux is (a) $\phi=0$, (b) $\phi=\phi_0/5$, and (c) $\phi=2\phi_0/5$. We have chosen $\epsilon_A=2$ and $\epsilon_B=0$ with $t=1$. The AVDOS has been plotted within the range zero to two.

of the magnetic flux. This control over the proximity of the degenerate localized level and a subband can be utilized to simulate an extrinsic semiconductorlike behavior. For example, let us refer to the case in which $\epsilon_A=2$ and $\epsilon_B=0$ and fix the Fermi level at $E=2$ (i.e., all states from the bottom of the left (valence) band up to $E=2$ are filled up at $T=0$ K). The strongly degenerate level is pinned at $E=2$. If the magnetic field is small then the energy gap between the localized level at $E=2$ and the bottom of the conduction band (the right subband) is small enough for electrons to bridge. The system now behaves as an n-type semiconductor. By reverting to the case of $\epsilon_A=-2$ we can simulate a p-type semiconductorlike behavior observed by the same diamond chain. In this case the localized level is pinned at $E=-2$ and we need to fix the Fermi level at the top of the valence band so that electrons can jump into unoccupied levels above creating holes in the valence band. It should be noted however that with increasing flux the gap width increases, and hence the probability of electrons crossing over to any one of the subbands decreases.

In Fig. 4 we present the variation in the concentration of electrons (holes) at finite temperatures in the conduction (valence) bands for $\epsilon_A=2$ and -2, respectively. With flux increasing from zero the carrier concentration (electron or hole) diminishes.

The applicability of the above physics depends on whether such features are exhibited by systems with a finite size as well. In order to check this we have calculated the density of states and conductance of a 20-plaquette chain. To

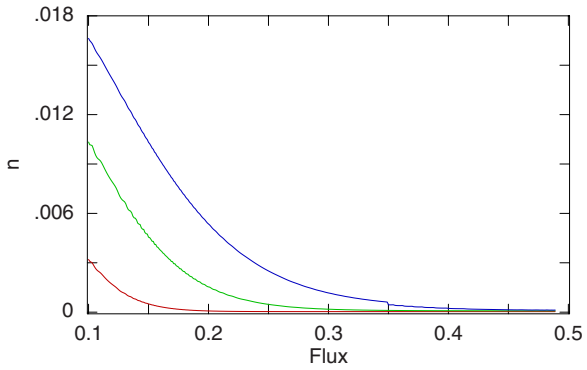

FIG. 4. (Color online) Variation in the electron concentration n as a function of the flux ϕ. The red, green, and blue curves correspond to the temperatures $k_BT=0.5$, 1, and 1.5 respectively, with k_B being the Boltzmann constant.

calculate the conductivity, the system is connected between two metallic electrodes, viz., the source and the drain (Fig. 5), described by the standard tight-binding Hamiltonian and parametrized by a constant site potential ϵ_0 and nearest-neighbor hopping integral t_0. The hopping integral between the source and the system is τ_S while it is τ_D between the system and the drain. Throughout the calculation we choose the units where $c=e=h=1$. For low bias and low temperature one calculates the conductivity using the single-channel Landauer formula[17] $g=(2e^2/h)\mathcal{T}$, where the transmission coefficient $\mathcal{T}$ is given by[17] $\mathcal{T}=\mathrm{Tr}[\Gamma_S G^r \Gamma_D G^a]$. Γ_S and Γ_D correspond to the imaginary parts of the self-energy due to the coupling of the diamond chain with the electrodes and G represents the usual Green's function. In Figs. 6 and 7 we have shown simultaneously the AVDOS and the conductance spectra. Figure 6 illustrates the symmetric case with $\epsilon_A=\epsilon_B=0$. With zero flux, the system exhibits oscillating conductance profile with resonance peaks. As the flux becomes nonzero and increases in value, the conductance windows occupy the regions corresponding to the two subbands at the flanks and shrink in width as the flux increases toward the half-flux quantum. Figure 7 depicts a similar qualitative feature but now with an asymmetric conductance profile as the potentials ϵ_A and ϵ_B are different.

Before we end, it may be mentioned that whether an array of such plaquettes will behave as an insulator or will have a metallic character in the absence of an external magnetic field, depends on the geometry of the unit cells. For example, with an array of identical triangular plaquettes a gap already exists in the middle of the spectrum even when the external magnetic field is zero. Thus such a triangular array will have an insulating character at $T=0$ K and at zero flux. However,

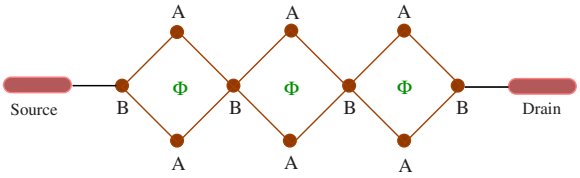

FIG. 5. (Color online) Schematic view of a finite diamond chain attached to two metallic electrodes.

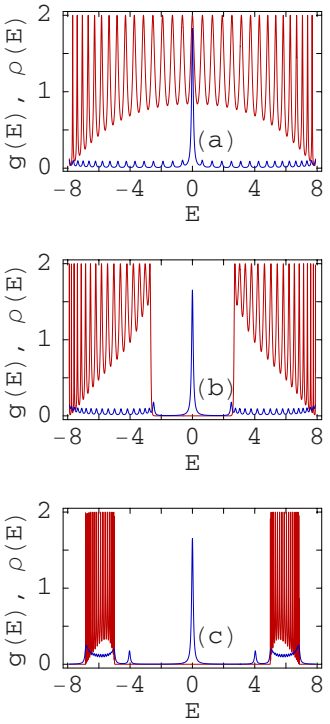

FIG. 6. (Color online) g-E (red color) and ρ-E (blue color) curves for a 20-ring chain. (a) $\phi=0$, (b) $\phi=0.2$, and (c) $\phi=0.4$. Other parameters are $\epsilon_A=\epsilon_B=0$, $t=3$, $\epsilon_0=0$, $t_0=4$, and $\tau_S=\tau_D=2.5$.

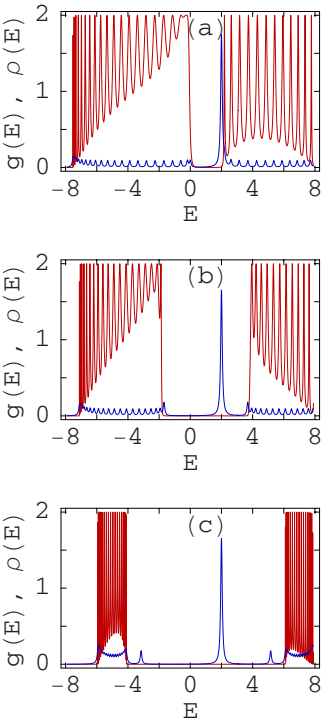

FIG. 7. (Color online) g-E (red color) and ρ-E (blue color) curves for a 20-ring chain. (a) $\phi=0$, (b) $\phi=0.2$, and (c) $\phi=0.4$. Other parameters are $\epsilon_A=2$, $\epsilon_B=0$, $t=3$, $\epsilon_0=0$, $t_0=4$, and $\tau_S=\tau_D=2.5$.

by changing the site potentials one can generate strictly localized levels inside the gap and can again have the n- or p-type semiconducting behavior as discussed earlier in respect of the diamond plaquette array.

Finally, in view of the potential application of the networks as a device we would like to point out that the qualitative features presented here should remain valid even at finite temperature ($\sim$300 K) since the broadening of the energy levels of the diamond array due to its coupling with the electrodes will be much larger than that of the thermal broadening.[17]

[1] A. Aharony, O. Entin-Wohlman, Y. Tokura, and S. Katsumoto, Phys. Rev. B **78**, 125328 (2008).
[2] A. Aharony, O. Entin-Wohlman, Y. Tokura, and S. Katsumoto, Proceedings of Frontiers of Quantum and Mesoscopic Thermodynamics FQMT08, arXiv:0812.2359v1 (unpublished).
[3] A. Rodríguez, F. Domínguez-Adame, I. Gómez, and P. A. Orellana, Phys. Lett. A **320**, 242 (2003).
[4] P. A. Orellana, F. Domínguez-Adame, I. Gómez, and M. L. Ladrón de Guevara, Phys. Rev. B **67**, 085321 (2003).
[5] A. L. Yeyati and M. Büttiker, Phys. Rev. B **52**, R14360 (1995).
[6] M. E. Torio, K. Hallberg, S. Flach, A. E. Miroshnichenko, and M. Titov, Eur. Phys. J. B **37**, 399 (2004).
[7] E. Buks, R. Schuster, M. Heiblum, D. Mahalu, V. Umansky, and H. Shtrikman, Phys. Rev. Lett. **77**, 4664 (1996).
[8] A. Fuhrer, P. Brusheim, T. Ihn, M. Sigrist, K. Ensslin, W. Wegscheider, and M. Bichler, Phys. Rev. B **73**, 205326 (2006).
[9] K. Kobayashi, H. Aikawa, A. Sano, S. Katsumoto, and Y. Iye, Phys. Rev. B **70**, 035319 (2004).
[10] M. Popp, D. Frustaglia, and K. Richter, Nanotechnology **14**, 347 (2003).
[11] P. Földi, O. Kálmán, M. G. Benedict, and F. M. Peeters, Nano Lett. **8**, 2556 (2008).
[12] D. Bercioux, M. Governale, V. Cataudella, and V. M. Ramaglia, Phys. Rev. Lett. **93**, 056802 (2004).
[13] D. Bercioux, M. Governale, V. Cataudella, and V. M. Ramaglia, Phys. Rev. B **72**, 075305 (2005).
[14] J. Vidal, B. Doucot, R. Mosseri, and P. Butaud, Phys. Rev. Lett. **85**, 3906 (2000).
[15] B. Doucot and J. Vidal, Phys. Rev. Lett. **88**, 227005 (2002).
[16] B. W. Southern, A. A. Kumar, and J. A. Ashraff, Phys. Rev. B **28**, 1785 (1983).
[17] S. Datta, *Electronic Transport in Mesoscopic Systems* (Cambridge University Press, Cambridge, 1997).